TCR binding to peptide-MHC complex acts as a drawbridge for CD3 cross-membrane signaling

Floris J. van Eerden[a*#], Aalaa Alrahman Sherif[b#], Mara Anais Llamas-Covarrubias[b] & Daron M. Standley[b*]

[a]Immunology Frontier Research Center, Osaka University, 3-1 Yamadaoka, Suita, Japan
[b]Research Institute for Microbial Diseases, Osaka University, 3-1 Yamadaoka, Suita, Japan

[*]Corresponding author
[#]Equal contribution

E-mail: Floris van Eerden fvaneerden@ifrec.osaka-u.ac.jp
Daron Standley standley@biken.osaka-u.ac.jp

Abstract

The mechanism of T cell triggering upon engagement with a peptide-MHC (pMHC) complex remains a challenging problem. In order to observe structural and dynamics changes in the T cell receptor (TCR) upon pMHC binding, we carried out coarse grained molecular dynamics simulations of TCR-only and TCR-pMHC systems starting from a recently solved cryo-EM structure of the TCR and CD3. The simulations were performed in biological membranes for an aggregated length of 2 ms. We observed that, while unengaged TCRs adopted conformations that bent and restricted the dynamics of the CD3s, the pMHC-bound TCRs adopted elongated conformations that allowed the CD3s to diffuse more freely. In this way, the TCR-pMHC pair acted as a "drawbridge", licensing CD3 dynamics, resulting in signal transmission across the plasma membrane. We then identified a conserved pair of Glycine residues in the hinge region of the TCR beta chain that facilitates the transition from the CD3-engaged to the pMHC-engaged states. All-atom simulations of TCRs whose hinge residues were rigidified by substituting Glycine with Proline weakened CD3 engagement. Consistently, we found that reporter cells with rigidified TCR hinges were hyperresponsive to pMHC stimulation in the early (2-4 hour) phase of T cell activation. These results suggest a model where TCR triggering is facilitated by increased CD3 dynamics, which, in turn, is enabled by TCR-pMHC engagement, rigidification of the TCR hinge, or both.

Introduction

T cell receptors (TCRs) play a central role in adaptive immunity by recognizing peptide antigens presented by major histocompatibility complex (MHC) molecules. The binding of agonistic, but not antagonistic, peptide-MHC (pMHC) complexes results in TCR triggering, a set of biochemical changes in the cytoplasmic regions of the CD3 complex (van der Merwe and Dushek, 2011) that can subsequently lead to T cell activation. The effector functions of activated T cells range from the killing of infected cells to inhibition of immune responses, to establishment of memory of specific peptide antigens. In line with their importance, TCRs have been intensively studied over

the last several decades; however, the mechanisms linking pMHC engagement with TCR triggering remain elusive.

In the last decade, a number of models of T cell activation and TCR triggering have been proposed, each emphasizing different aspects of the phenomena. The relationship between initial pMHC engagement and cytoplasmic signaling is treated by the *mechanosensor model*. In this model, TCRs discriminate agonistic from antagonistic pMHCs via catch bond formation (Sokurenko et al., 2008) (Zhu et al., 2019) (Feng et al., 2018; Hwang et al., 2020), which transfers force from the pMHC-TCR interface to the TCR-CD3 interface via the FG loop on the TCR (Das et al., 2015; Kim et al., 2009). Alternatively, the *kinetic proofreading* model emphasizes that pMHC-TCR complex lifetimes, rather than forces per se, are critical for distinguishing agnostic from antagonistic pMHCs (Lo et al., 2019). The *TCR bending mechanosignal model* argues that TCR-pMHC engagement results in changes in membrane curvature that promote conformational changes in the receptors that are transmitted to the cytoplasmic side (Al-Aghbar et al., 2022). Finally, in the *allosteric relaxation* model TCR-pMHC binding results in decoupling of interactions between TCR and CD3ζ (Rangarajan et al., 2018; Brazin et al., 2018; Lanz et al., 2021). While the models differ in detail, each requires a yet to be defined mechanical communication between the TCR and CD3 that is transmitted through the membrane. The TCR-CD3 linkage is crucial, since CD3s, but not TCRs, contain cytoplasmic immunoreceptor tyrosine-based activation motifs (ITAMs), which become phosphorylated upon activation.

On the cytoplasmic side, the *ITAM sequestration model* argues that the CD3 ITAMs are buried in the membrane in the resting state but, upon the proper extracellular signal, become exposed to the cytoplasmic lymphocyte-specific protein tyrosine kinase (Lck), whereupon a downstream signaling cascade occurs (Xu et al., 2008; Aivazian and Stern, 2000). Other models, including *kinetic segregation* (Nika et al., 2010; Davis and van der Merwe, 2006) and *aggregation* (Saito and Yokosuka, 2006; Cai et al., 2018) emphasize morphological changes in the synapse that forms between the engaged T cell and APC. Other studies have reported that individual TCRs can become triggered (Brameshuber et al., 2018), suggesting that there is merit in learning from simple TCR-pMHC systems.

In 2019, the first full-length structure of a TCR with CD3s was determined by single particle cryo-EM (Dong et al., 2019). Interestingly, this structure revealed that the extracellular domain (EC) of the TCR is bent 144° with respect to the membrane normal. This observation raised the question of whether the angle between the TCR EC and transmembrane domain (TM) is dynamic. Molecular dynamics studies based on the complete TCR structure in a membrane demonstrated that the TCR is indeed flexible and that the TCR headgroup can adopt a range of different conformations (Prakaash et al., 2021; Pandey et al., 2021).

These recent findings raise new questions. Of particular interest is how pMHC engagement affects the dynamics of the TCR. Such dynamics may shed much needed light on the nature of the communication between the TCR and CD3 in T cell triggering. To this end, we carried out extended molecular dynamics simulations of two systems: a "TCR-only" system (Figure 1A), which consisted of only the TCR CD3 complex embedded in a membrane, and a "TCR-pMHC" system, consisting of two opposing membranes: one containing a pMHC and the other containing a TCR CD3 complex (Figure 1B). The cumulative simulation time for each system was 1 ms. Although there have been previous studies of a TCR in complex with a pMHC (Wan et al., 2008; Bello and Correa-Basurto, 2016; Alba et al., 2020), to our knowledge, this is the first attempt to compare free and pMHC-engaged TCRs based on the complete cyro-EM structure (Dong et al., 2019), which critically contains the CD3s.

Consistent with earlier work, we observed a wide range of conformational states for the TCR-only system. As might be expected, the TCR-pMHC system was more restricted. However, what was surprising is that pMHC engagement was associated with significantly larger dynamic motions in the CD3 coreceptors. In our simulations, TCR-pMHC engagement allowed the CD3s to move around the TCR. Importantly, these simulations did not contradict key evidence of previously-proposed triggering models. For example, in agreement with the mechanosensor and kinetic proofreading models, we observed a critical role of the FG loop on CD3 dynamics. Our simulations also recapitulated key findings of the allosteric relaxation model. Taken together, our findings show that dynamics is critical to understand the communication between the extracellular and cytoplasmic events that occur in TCR triggering.

Results

Description of the simulation systems

To study the dynamics of the TCR under resting and pMHC-engaged conditions, two systems were constructed: A TCR-only system, in which a single TCR was embedded in a POPC bilayer (Figure 1A) and a TCR-pMHC system (Figure 1B). The later system was composed of two opposing POPC bilayer slabs; the lower representing the T cell membrane and containing a TCR, and the upper representing the APC membrane in which a pMHC was embedded. The TCR in the simulations was a fusion between the complete TCR cryo-EM structure (PDB ID 6jxr) and a crystal structure of a pMHC-bound TCR (PDB ID 3qiu), which lacked the TCR TM (Dong et al., 2019) (Newell et al., 2011). Harmonic potentials based on the crystal structure were used to bind the TCR to the pMHC; the potentials were applied in a stepwise manner during 1.5 µs preparatory simulations to let the system slowly adjust (Figure S1). A pore was created in the APC membrane in order to allow the flow of solvent between the two membrane compartments, which was required in order for the distance between the APC and T cell membranes to change naturally. For each system, one hundred 10 µs production runs were performed, totaling 1 ms per system.

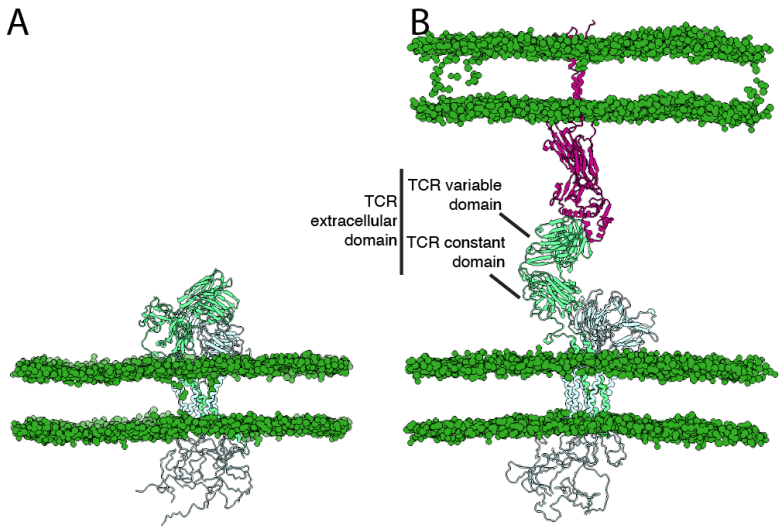

Figure 1: The TCR only and TCR-pMHC simulations systems. Snapshots of the TCR-only (A) and TCR-pMHC (B) simulation systems. The TCR is in lime, CD3s in cyan, pMHC in purple and lipid headgroups in green. Note that in the TCR-pMHC channel a pore is present in the upper membrane to allow the flow of solvent between the two compartments, which is why headgroup beads are visible in the membrane interior. Solvent and lipid tails are

not shown for clarity. In panel B the TCR variable (V) and TCR constant (C) domains are indicated. The TCR extracellular domain (EC) encompasses the variable and constant domains.

CD3 epsilon chains exhibited a wider range of motion upon TCR-pMHC engagement.

Iso-occupancy surfaces were calculated to study the distribution on the CD3 epsilon chains in the simulations. The CD3 epsilon chains in the TCR-pMHC simulations sampled a larger area around the TCR compared to the TCR-only simulations (Figure 2). The iso-occupancy surface of the CD3 epsilon chains in the TCR-only simulations had a clear minimum close to the position of the CD3ζ chains (Figure 2A), in contrast the CD3 epsilon chains in the TCR-pMHC simulations sampled the region around the TCR completely (Figure 2B). Interestingly the TCR-only iso-occupancy surface was not symmetric, with the occupancy being especially low around the CD3ζ chain that is next to CD3γ (hereafter CD3ζ^{γ}).

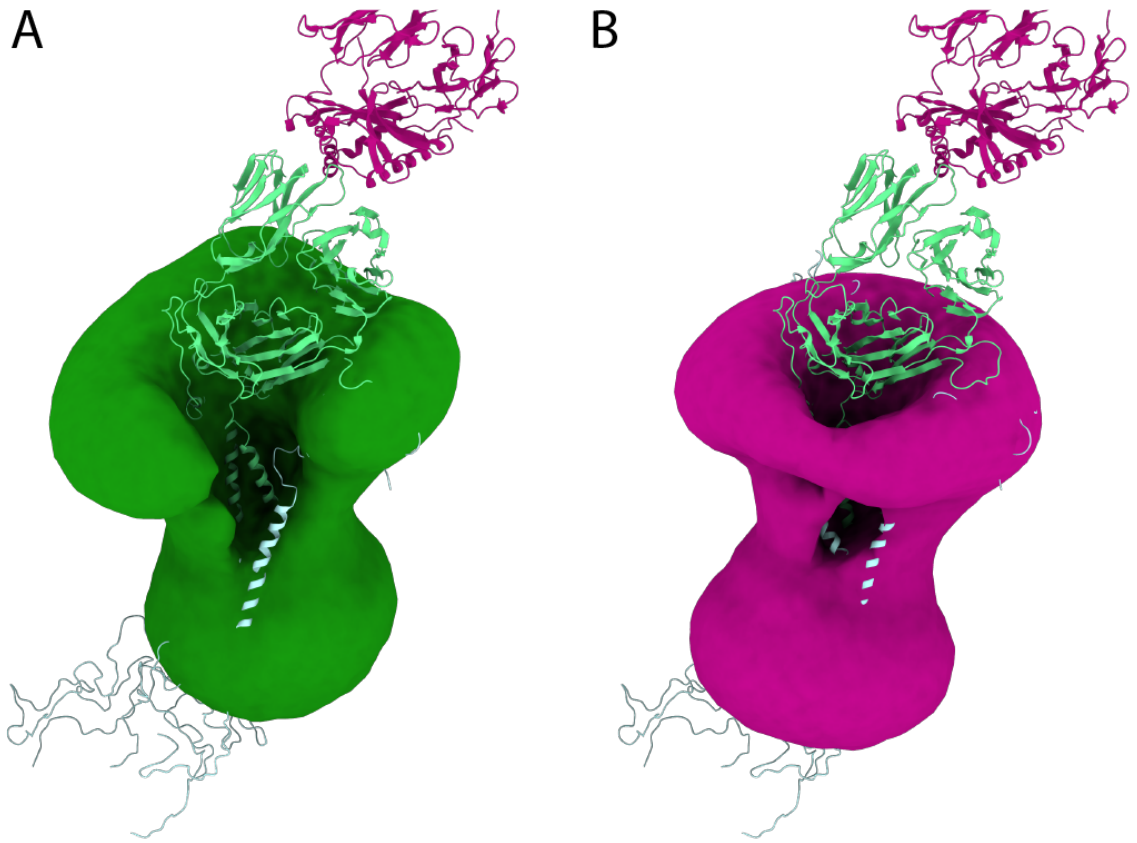

Figure 2: Iso-occupancies of CD3$\varepsilon^{\gamma}\varepsilon^{\delta}$ around the TCR αβ chains. Iso-occupancy of CD3$\varepsilon^{\gamma}\varepsilon^{\delta}$ in the TCR-only simulation is shown in green (panel A), and in purple for the TCR-pMHC simulation (panel B). The TCR is colored in lime, CD3s in cyan (mostly obscured by the iso-surfaces) and pMHC in purple.

pMHC engagement resulted in fewer contacts between the CD3s and the TCR variable domain

To get a better understanding of the reasons for the difference in CD3 distribution in the simulations systems, the contacts between the CD3 and the TCR chains were analyzed. There were clear differences in the quantity and type of contacts between the TCR and the CD3s in the TCR-only and TCR-pMHC simulations, especially for contacts involving the TCR variable domain (V) (Figure 3 and Figure S2). The epsilon chain in contact with CD3γ (hereafter CD3ε^{γ}) (Figure 3A) and the CD3γ chain (Figure 3B) were consistently in contact with the TCR V in the TCR-only simulations; however, these interactions virtually disappeared in the TCR-pMHC simulations.

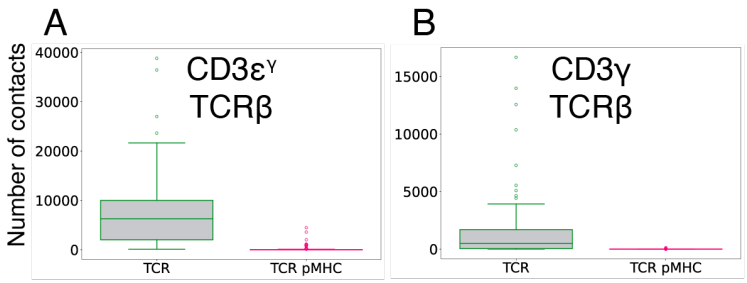

Figure 3: TCR CD3 contacts. The number of contacts between the TCRβ variable domain and the indicated CD3 chains in the TCR-only (green box plots) and TCR-pMHC (pink box plots). Note that the y-axis varies between the three plots. Please refer to Figure S2 for the contacts specified per residue.

TCR straightens upon pMHC engagement

The TCR adapted qualitatively different conformations upon pMHC binding, as measured by the angle between the TCRβ transmembrane domain (TM) and extracellular domain (EC) (Figure 4). In the TCR-only system, in which the TCR EC folded over the CD3s (Figure 1A), the TCR adopted predominantly bent conformations (smaller angles), with a peak in the distribution at 104°. Such bending was observed in previous simulations of the same starting structure (Pandey et al., 2021). In contrast, the TCRs in the TCR-pMHC system, for which the many interactions with CD3 were broken, tended to adopt an extended and open conformation (larger angles, with the peak of the distribution at 150°) where the TCR EC tilted away from the CD3 EC domains (Figure 4 and Figure 1B). The TCR-pMHC simulations also sampled a narrower distribution of angles, with a full-width at half-maximum (FWHM) of approximately 30°, than the TCR-only simulation (FWHM 40°).

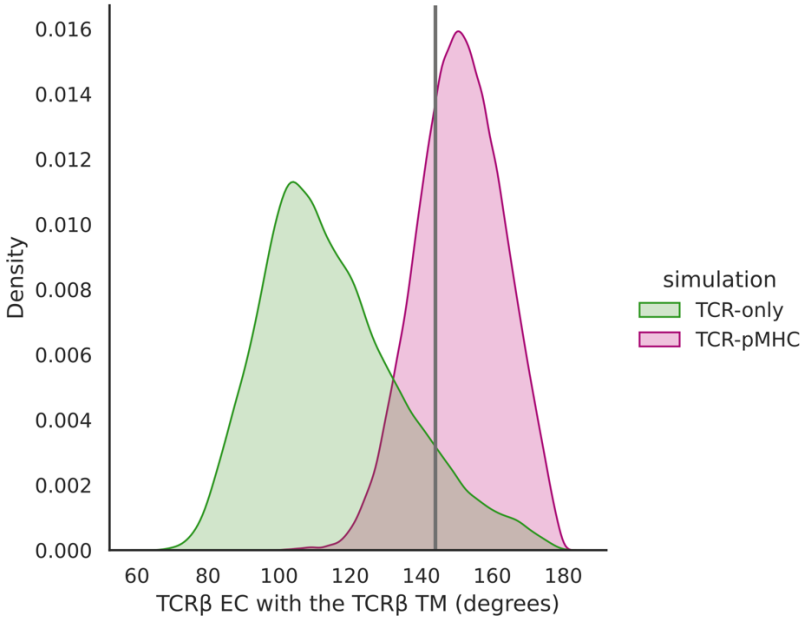

Figure 4: Angle distributions of the TCRβ EC with the TCRβ TM. Angle distribution of the TCR-only (lime) and TCR-pMHC (pink) systems. The angle of the cryo-EM structure (vertical line) was 144°.

TCR acts as drawbridge

When combining these three observations, a mechanism emerges in which the TCR adopts a bent conformation in the "TCR-only" simulations, with the TCR V binding to the CD3s, thereby hindering their movement. Upon pMHC binding, the TCR adopts a more extended conformation, which breaks the bonds between the TCR V region and the CD3s, subsequently allowing them to diffuse around the TCR. The TCR thus acts as a "drawbridge", in which the opening of the bridge (pMHC binding) allows the passing of the CD3s, leading to increased dynamics across the membrane (Figure 5). We hypothesize, over time, such unrestricted dynamics results in rearrangements of the ITAMS, ultimately resulting in their phosphorylation.

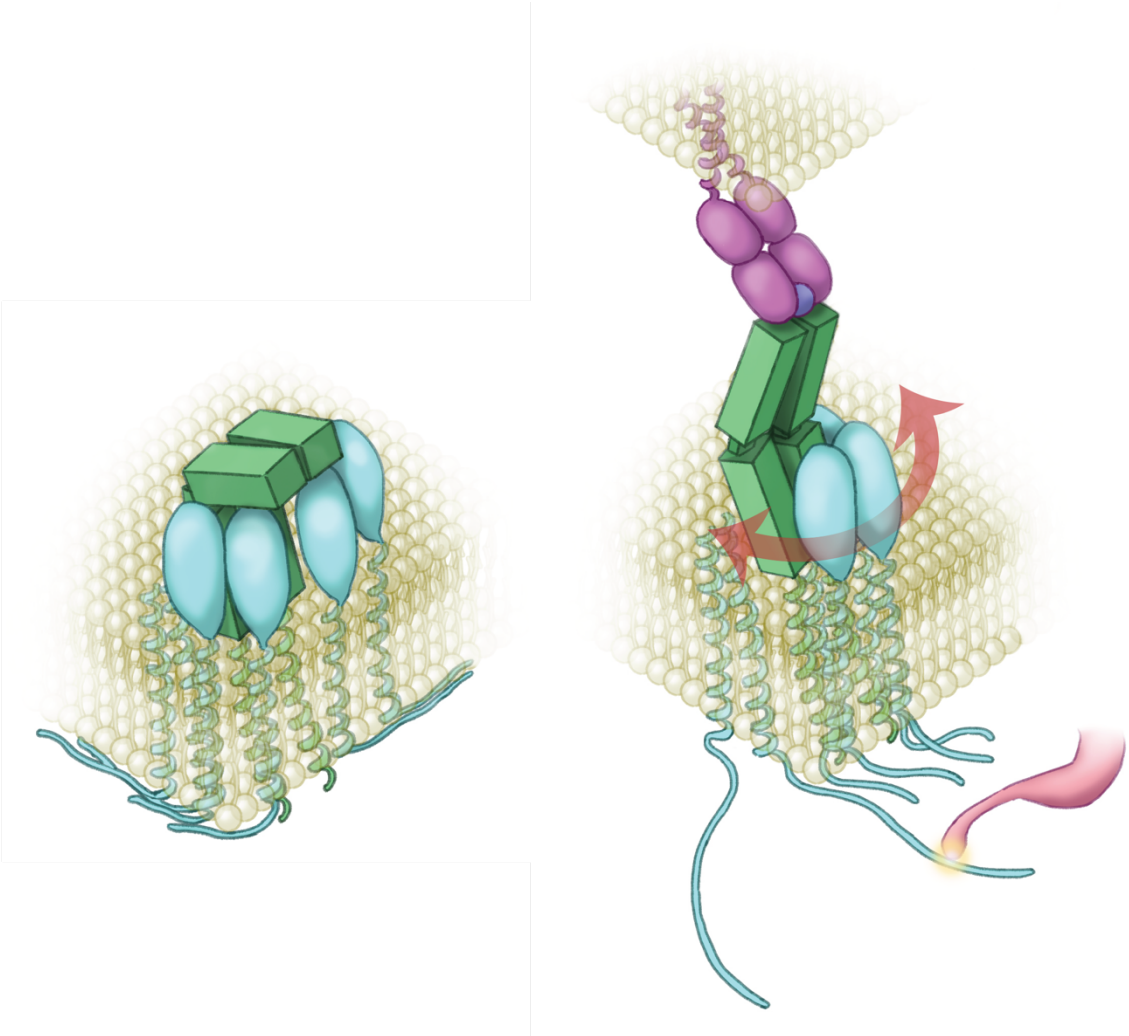

Figure 5 TCR-pMHC binding acts as a drawbridge for the CD3s. In the left panel the unengaged TCR is bent over the CD3s, preventing their diffusion. Upon pMHC binding (right panel), the TCR straightens, resulting in release of the CD3s, allowing their diffusion around the TCR. This freedom facilitates exposure of cytoplasmic tails from the membrane, licensing phosphorylation of the ITAMs.

Role of the TCRβ FG loop

Long range perturbations were observed in previous experimental studies of the TCR upon pMHC binding, notably in three key regions: the TCRα AB loop; the TCRβ H3 helix; and the TCRβ FG loop (Mariuzza et al., 2020; Natarajan et al., 2017; Rangarajan et al., 2018). In agreement with

these experimental observations, differences in these regions upon pMHC binding were observed in our simulations as well. Both the TCRα AB loop and the TCRβ H3 helix exhibited increased interactions with one of the CD3 epsilons upon pMHC binding. The TCRα AB loop contacted the CD3 epsilon of the CD3εγ dimer (hereafter CD3ε^{γ}) predominantly in the TCR-pMHC simulations (Figure 6A), while the TCRβ H3 helix made more contacts with the CD3 epsilon of the CD3εδ dimer (hereafter CD3ε^{δ}) in the TCR-pMHC simulation (Figure 6B). The TCRα AB loop and the TCRβ H3 helix are located out of reach from CD3ε^{γ} and CD3ε^{δ}, respectively, in the cryo-EM structure; this made interactions between these regions unlikely to occur in the TCR-only systems, in which the CD3 movement is restricted. Upon pMHC binding, however, the interactions between the TCR EC and the CD3s, were broken, resulting in increased movement of the CD3 epsilon chains which could subsequently interact with previously inaccessible areas of the TCR.

Experiments and simulations suggested that the TCRβ FG loop has an important role in TCR triggering and that the TCR FG loop dynamics changes upon pMHC binding (Kim et al., 2009; Das et al., 2015; Rangarajan et al., 2018). We observed that the TCRβ FG loop contacted CD3ε^{γ} in the TCR-only simulations more than in the TCR-pMHC simulations (Figure 6C). Inspection of the trajectory showed that the TCRβ FG loop blocked the diffusion of the CD3εγ dimer proximate to TCRβ. In the pMHC simulations, the TCRβ FG loop moved up and allowed diffusion of the CD3εγ.

These data suggest that the TCRβ FG acts as a break on the system, preventing the diffusion of the CD3εγ dimer when the TCR is unbound. This also explains the asymmetry observed in the CD3 epsilon distributions in the TCR-only simulations (Figure 2A). The iso-occupancy maps in the TCR-only simulation lack density specifically around CD3ζ^{γ}, while there is clear density around the CD3ζ chain that is next to CD3ε^{δ} (hereafter CD3ζ^{ε}). While the positioning of the CD3s around the TCR is fairly symmetric, the TCRα chain lacks the equivalent of the TCRβ FG loop. This grants CD3εδ the possibility to occasionally move alongside the TCRα chain, while an equivalent movement by CD3εγ is blocked by the TCRβ FG loop. This also can be seen the contacts between TCRα and the CD3 epsilon chains (Figure S3) where the difference between the TCR-only and TCR-pMHC simulations is much smaller compared to the difference in contacts between TCRβ and CD3εγ (Figure 3). Consistently, a reduction in TCR CD3ζ interactions has been observed upon

pMHC binding in DDM stability assays (Lanz et al., 2021). In line with this evidence, we observed a reduction in the contacts between the CD3ζ chains and TCRβ upon pMHC binding (Figure S4).

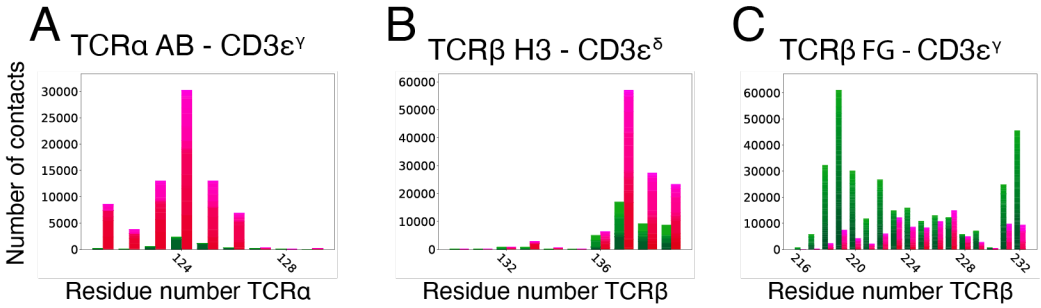

Figure 6: Cumulative TCR – CD3 contacts. Contacts between CD3s and the TCRα AB loop (A), TCRβ H3 helix (B) and the TCRβ FG loop (C) in the in TCR-only (green bars) and TCR-pMHC simulations (red bars). Contacts are summed over all simulations and are shown as gradients, where each step in the gradient represent the contacts in a single simulation. Residue numbers of the TCRα or TCRβ chains are shown on the x-axis. Note that the y-axis varies between the plots.

Critical role of hinge residues in TCR triggering

Given the importance of TCR conformational changes in CD3 dynamics, we next investigated potential hinge residues in the TCR. We identified a highly conserved GxxG motif in the linker region between the immunoglobulin and transmembrane regions of TCR beta chain. Whereas the TCR alpha chain contains a long, flexible linker, the TCR beta chain is quite short. Moreover, the two linkers are attached by a disulfide bond, implying that global changes in the TCR angle depend on these two glycine residues. We reasoned that, if TCR-CD3 coupling requires TCR bending, rigidification of the hinge should affect CD3 dynamics, and, by extension T cell triggering. Indded, when we performed all-atom MD simulations of TCR mutants where the Glycines were substituted with more rigid Prolines, the CD3s exhibited a wider range of movement than when they were paired with WT TCRs.

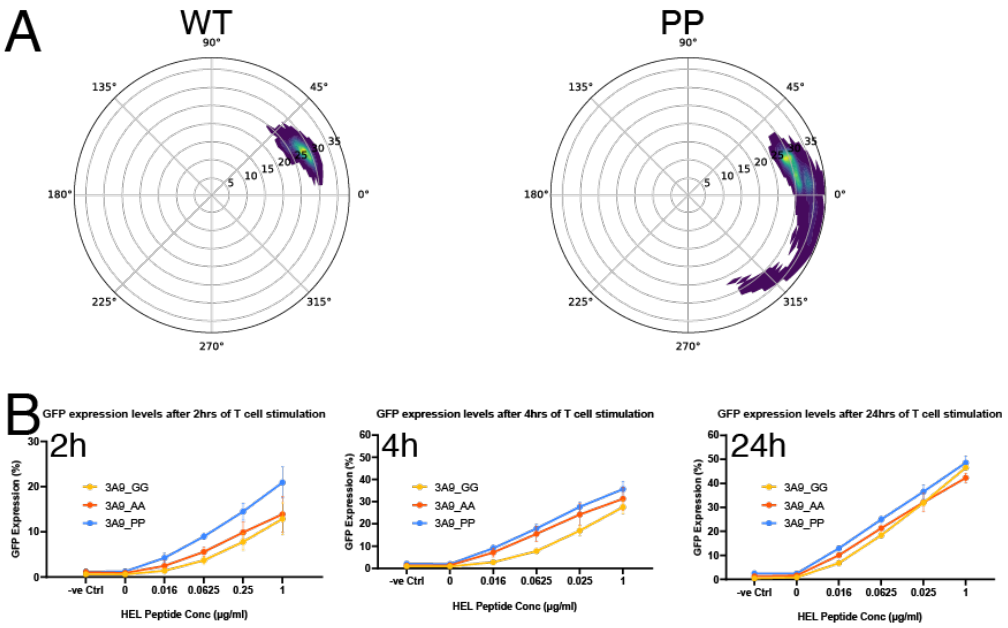

Figure 7: Hinge rigidification results in hyperresponsive T cells. All-atom MD simulations (A) for WT and "rigidified" (GG->PP) TCR mutants indicated that the movement of CD3ε^{γ} (represented as densities in a 2D plane about the TCR) increased in the rigidified (PP) simulations compared to WT. Consistently, when NFAT reporter cells were transfected with WT (GG), AA or PP mutant TCRs, the cells with the rigidified (PP) TCRs were hyperresponsive to pMHC stimulation after 2 hrs. Moreover, the difference between mutant and WT cells decreased after 4 and 24 hrs, respectively.

T cells with rigidified hinges are hypersensitive to pMHC stimulation

To test whether TCR-CD3 coupling depends on the hinge residues, we expressed GG->AA and GG->PP mutants and measured T cell responses to pMHC stimulation. We observed that rigidification resulted in T cell hypersensitivity in the order PP > AA > GG 2 hours after stimulation. Interestingly, the effect was reduced at 4 hours, and disappeared by 24 hours, suggesting that the hinge flexibility is responsible for initial triggering events, but when given enough time, large-scale interactions leading to T cell activation are feasible even in mutant TCRs.

Discussion

The critical role of T cells in host immunity has inspired decades of research into TCR structure and function. In spite of this vast volume of work, the molecular mechanism of TCR-mediated signal transduction from the pMHC to the CD3 ITAMs remains an open question. Even if we take for granted that agnostic pMHC complexes induce sufficient force or persist for a requisite threshold of time, a complete understanding of TCR triggering must also include some form of coupling between the TCR and the CD3s. Without this coupling, the causes of triggering events in the cytoplasm remain a mystery.

It has been proposed that catch bonds effect the dynamics of the TCR and, by extension, the TCR-CD3 interface. Recent NMR studies (Rangarajan et al., 2018; Natarajan et al., 2017) support this line of reasoning. Specifically, three regions (TCRβ FG, TCRα AB, and TCRβ H3) have been shown to exhibit chemical shift signal perturbations upon pMHC binding, implying that pMHC-TCR interactions mediate long-range changes in TCR structure, dynamics, or both (Beddoe et al., 2009). The recent cryo-EM structure of the TCR CD3 complex afforded an opportunity to examine differences in the structure and dynamics in the TCR-only and TCR-pMHC systems by molecular dynamics.

Our simulations consisted of two membrane-embedded TCR CD3 complexes with and without a second pMHC system. Two recent molecular dynamics studies of TCR-only systems based on the same cryo-EM structure, have recently been reported, allowing us to compare our TCR-only simulations and assess the generalizability of our observations (Prakaash et al., 2021) (Pandey et al., 2021). Three main takeaways were consistent in all three molecular dynamics studies:

1) The pMHC-unbound TCR was highly dynamic, sampling a wide range of conformations
2) These conformations included states with even greater bending of the EC with respect to the membrane than in the initial cryo-EM structure

3) There was tight coupling between TCR and CD3 chains that were mediated by several regions in the TCR, including the FG loop

With these qualitative validations of our TCR-only simulations in hand, we next scrutinized the TCR-pMHC simulations, with the goal of identifying differences in the ITAM-containing CD3 chains. MD studies performed prior to release of the full TCR cryo-EM structure suggested that the TCR itself rigidified upon pMHC binding (Rangarajan et al., 2018). We observed that, indeed, fluctuations in the angle of the TCR headgroup with the plasma membrane were reduced in the TCR-pMHC system as compared to the TCR-only system, with a drop in the full-width at half maximum of ~10 degrees (Figure 4). However, while the TCR became less flexible, the CD3s became more dynamic in the TCR-pMHC system. We rationalized these differences in terms of a "drawbridge" effect of the TCR and pMHC: when the TCR straightened to engage with the pMHC, it removed a brake on the CD3 chains, allowing them to diffuse around the TCR (Figure 5). The coupling between TCR and CD3s (mediated in part by the FG loop) was reduced significantly (Figure 3). This key observation nicely integrates the mechanosensor, allosteric relaxation and ITAM sequestration models into a coherent whole: Catch bonds hold the TCR-pMHC together, which decouples the TCR from the CD3s (in particular CD3εγ), licensing CD3 dynamics, ultimately leading to ITAM phosphorylation. We next identified hinge residues in the TCR beta chain that allow the TCR to engage with CD3. When these residues were rigidified by transgenic expression of mutant TCRs in reporter cells, the cells became hyperresponsive at early (2-4 hr) timepoints (Figure 7). Therefore, TCR conformational changes can act to restrict or free CD3 dynamics. This is a robust mechanism that is not dependent on specific details of the TCR CDRs. Rather, any TCR-pMHC interface of sufficient lifetime to allow CD3 diffusion underneath the drawbridge can lead to triggering.

Acknowledgments

Simulations were performed using the Research Center for Computational Science, Okazaki, Japan (Projects: 20-IMS-C116, 21-IMS-C116 and 22-IMS-C116) and the TSUBAME3.0 supercomputer at Tokyo Institute of Technology. The authors wish to thank Misaki Ouchida for creating the illustration explaining the Dynamic Drawbridge model.

Methods

Our interest in this project was to study a conventional TCR-MHC complex, but the extracellular part of the TCR electron densities of the De Dong structure have been fitted on the coordinates of an atypical natural killer TCR. For this reason, we fused the structure of the De Dong et al. (PDB ID 6jxr) (Dong et al., 2019) with the structure of a conventional TCR from Newell et al. (PDB ID 3qiu) (Newell et al., 2011). For the CD3s and the transmembrane part of the TCR the structure of De Dong was used. The ITAM fragments were not present in the structure of De Dong and were modeled according to the murine sequence (see below). The structure by Newell et al served as the basis of MHC and of the extracellular parts of the TCR. It should be noted that the structure by De Dong is human, while the Newell structure and the modeled ITAM fragments are murine.

MHC

The structure from Newell et al lacks the MHC transmembrane helices, were modeled using HHpred (Zimmermann et al., 2018) and Pymol (Schrödinger, 2010). In order to obtain a realistic

orientation of the two MHC transmembrane helices, a 10 µs coarse grained molecular dynamics simulation of the two helices embedded in a POPC bilayer composed out of 221 lipids was performed with the martini 3 force field (version v.3.0.4.26). The modeled atomistic helices were subsequently fitted on the simulated structures and connected to the soluble part of the MHC from Newell et al. using Modloop (Fiser and Sali, 2003). The epitope was restrained to the MHC using a number of harmonic potentials (Gromacs bondtype 6), see Table 4.

TCR

For the simulation a fusion of the structures of De Dong et al. and Newell et al. was created. From the structure of De Dong the CD3s were taken, and the transmembrane segments of the α and β chains, which correspond to residue numbers 224-273 for the α chain and resid 264-308 for the β chain. The soluble segments of the TCRαβ chains were taken from the structure of Newell et al., for the α chain residues 2-199 and for the β chain residues 2-244, please note that the residue numbering is according to the respective pdb files. The structures were fused using Pymol (Schrödinger, 2010) and Modloop (Fiser and Sali, 2003). One should note that the murine TCR has an extra disulfide bond between the TCR α and β subunits with respect to the human TCR, the cysteine bond between TCRα CYS156 and TCRβ CYS171 has no counterpart in the structure of De Dong.

Part of the missing and incomplete TCR and MHC residues were reconstructed using Spanner (Lis et al., 2011) and Pymol (Schrödinger, 2010), see Table 3. For a list of the residues that were included in the simulation, see Tables 1 & 2. ITAMs (immunoreceptor tyrosine-based activation motif) were modeled using Pymol. The TCR was coarse grained (see below), embedded in a membrane (see below) and a set of equilibration simulations was performed to equilibrate the ITAM chains.

Positioning of TCR and MHC

TCR and pMHC were carefully positioned on top of each other in preparatory 1.5 µs simulations. The TCR and MHC were embedded in opposing membrane slabs, which were separated by ~21 nm (GL1-GL1 bead distance) (Figure 1). A set of distance restraints based upon the Newell structure (PDB ID 3qiu) (Newell et al., 2011) was defined between TCR and pMHC (Table 6).

During the 1.5 μs docking simulation a low force constant of 1 kJ mol^{-1} nm^{-2} was used to prevent any deformations. During the docking simulation the TCR and pMHC were slowly pulled together by the distance restraints resulting in a bound TCR-pMHC structure (Figure S1). In the production simulations a higher force constant of 200 kJ mol^{-1} nm^{-2} was used to keep the pMHC properly bound to the TCR. In order to allow solvent flow between the two membrane compartments, which in turns allows the bilayers to move, a pore was created in the bilayer containing the MHC. The pore was created using two cylinder shaped inverted flat bottom position restraints (function type 2, shape g = 8 in Gromacs). The first restraint, which was used to create the actual pore, acted on POPC beads with a force constant of 1000 kJ mol^{-1} nm^{-2} and a radius of 2 nm. The second restraint with a force constant of 2000 kJ mol^{-1} nm^{-2} and a radius of 4 nm acting on the MHC backbone beads was to make sure the MHC TM did not diffuse into the pore. Note that the preparatory simulations were performed for each of the one hundred TCR-pMHC simulations independently.

T cell receptor + CD3s

Protein name (Chain ID in PDB file (6jxr/3qiu))	Residues in CG simulation	Section of ITAMs modelled	Residues in FG simulation
CD3ζ^{ε} (6jxr: A)	22-164	57-164	22-56
CD3ζ^{γ} (6jxr: B)	24-164	56-164	24-55
CD3δ (6jxr: D)	22-173	130-173	22-129
CD3ε^{δ} (6jxr: E)	33-180	138-180$^{\#}$*	33-155
CD3ε^{γ} (6jxr: F)	33-180	138-180$^{\#}$*	33-155
CD3γ (6jxr: G)	24-182	139-182	24-138
TCRα (6jxr: M/3qiu: C)$^{\$}$	2-249	-	2-249
TCRβ (6jxr: N/3qiu: D)$^{\$}$	2-293	290-293	2-289

MHC

Protein name (Chain ID in PDB file (3qiu))	Residues in CG simulation	Section of transmembrane helices modelled
MHCα (3qiu: A)	3-230	182-230
MHCβ (3qiu: B)	3-231	187-231

Epitope (3qiu: E)	2-14	-

Table 1: Residues included in the simulation. In the ITAM column numbers between brackets refers to the uniprot numbering [#]The CD3ε ITAM sequence length differs between mouse and human, numbers refer to mouse sequence. *Erroneously residue 181-189 of the CD3ε chains (TCR E and TCR F) were omitted during modelling and not included in the simulation. [$]Numbering scheme of 3qiu is used, chain C for TCR α and chain D for TCRβ.

	Residue numbering simulation	Residue Numbering 6jxr	Residue Numbering 3qiu	ITAMS modelled
TCRα				
extra cellular section	2-199	-	2-199	
Transmembrane section	200-249	224-273	-	
ITAM section	-	-	-	-
TCRβ				
extra cellular section	2-244		2-244	
Transmembrane section	245-288	264-308	-	
ITAM section	290-293	-	-	290-293

Table 2: Residues included in the simulation. In the ITAM column numbers between brackets refers to the uniprot numbering [#]The CD3ε ITAM sequence length differs between mouse and human, numbers refer to mouse sequence. *Erroneously residue 181-189 of the CD3ε^{δ} and CD3ε^{γ} chains (TCR E and TCR F) were omitted during modelling and not included in the simulation. [$]Numbering scheme of 3qiu is used, chain C for TCRα and chain D for TCRβ.

Protein	PDB ID	Chain	Residues
MHCβ	3qiu	B	105-113,134-135,165-170
TCRα	3qiu	C	145-146, 175-179, 187-199
TCRβ	3qiu	D	183-184, 219-220, 244
CD3ζ	6jxr	A	57 *modelled with Pymol
CD3ε	6jxr	F	156 *modelled with Pymol

Table 3: TCR and MHC residues which were reconstructed. Unless indicated, residues were reconstructed using Spanner (Lis et al., 2011).

MHC chain	MHC residue number	MHC residue	MHC bead	Epitope residue number	Epitope residue	Epitope bead	Equilibrium distance (nm)	Force constant (kJ mol^{-1} nm^{-2})
A	52	ALA	BB	2	ALA	BB	0.460	200
B	86	PHE	SC2	5	ILE	SC2	0.462	200
A	54	PHE	SC2	5	ILE	SC2	0.490	200
B	11	CYS	SC1	10	GLN	SC1	0.517	200

B	30	TYR	SC4	11	ALA	SC4	0.490	200
A	69	ASN	SC1	12	THR	SC1	0.507	200

Table 4: Harmonic potentials used to restrain the epitope in the MHC.

Protein	Residue number	Protein	Residue number
$^{+}$CD3ζ^{ε} (chain A)	32	CD3ζ^{γ} (chain B)	32
CD3δ	37	CD3δ	73
CD3δ	93	CD3δ	96
CD3ε^{δ} (chain E)	49	CD3ε^{δ} (chain E)	98
CD3ε^{δ} (chain E)	119	CD3ε^{δ} (chain E)	122
CD3ε^{γ} (chain F)	49	CD3ε^{γ} (chain F)	98
CD3ε^{γ} (chain F)	119	CD3ε^{γ} (chain F)	122
CD3γ	46	CD3γ	87
CD3γ	104	CD3γ	107
TCRα	22	TCRα	86
TCRα	131	TCRα	181
$^{+}$TCRα	156	TCRβ	171
$^{+}$TCRα	203	TCRβ	245
TCRβ	23	TCRβ	92
TCRβ	69	TCRβ	75
TCRβ	145	TCRβ	210
MHCα	105	MHCα	163
MHCβ	15	MHCβ	79
MHCβ	117	MHCβ	173

Table 5: Disulfide bonds present in the simulation. $^{+}$Inter-chain disulfide bond are modeled by a harmonic potential.

MHC chain	MHC residue number	MHC residue	MHC bead	TCR chain	TCR residue number	TCR residue	TCR bead	r_0 (nm)	r_1 (nm)	r_2 (nm)	Force constant (kJ mol^{-1} nm^{-2})
MHCβ	69	GLU	BB	TCRα	49	ALA	BB	0.593	0.693	3.093	200
MHCβ	77	THR	BB	TCRα	29	ARG	BB	0.482	0.582	3.682	200
MHCβ	84	GLU	BB	TCRα	65	LYS	BB	1.102	1.202	4.302	200
MHCα	57	GLN	BB	TCRβ	57	GLN	BB	0.788	0.888	3.988	200
MHCα	61	ALA	BB	TCRβ	33	PHE	BB	1.211	1.311	4.411	200
MHCα	75	GLU	BB	TCRβ	53	GLU	BB	1.800	1.900	5.000	200
MHCε	6	ALA	BB	TCRα	92	SER	BB	0.320	0.480	3.520	200
MHCε	11	ALA	BB	TCRβ	98	ASN	BB	0.429	0.529	3.629	200
MHCα	61	ALA	BB	TCRβ	55	LEU	BB	0.365	0.465	3.565	200
MHCα	64	ALA	BB	TCRβ	55	LEU	BB	0.560	0.660	3.760	200
MHCα	57	GLN	BB	TCRβ	55	LEU	BB	0.739	0.839	3.939	200
MHCα	64	ALA	BB	TCRβ	53	GLU	BB	0.649	0.749	3.849	200
MHCα	57	GLN	BB	TCRβ	53	GLU	BB	1.327	1.447	4.547	200
MHCα	61	ALA	BB	TCRβ	57	GLN	BB	0.917	1.067	4.167	200
MHCα	64	ALA	BB	TCRβ	57	GLN	BB	1.231	1.331	4.431	200
MHCα	57	GLN	BB	TCRβ	33	PHE	BB	1.421	1.521	4.621	200

MHCα	64	ALA	BB	TCRβ	33	PHE	BB	1.441	1.541	4.641	200
MHCα	64	ALA	BB	TCRβ	49	PHE	BB	0.899	0.999	4.099	200
MHCα	65	VAL	BB	TCRβ	49	PHE	BB	0.916	1.016	5.116	200
MHCα	61	ALA	BB	TCRβ	49	PHE	BB	0.843	0.943	5.043	200
MHCβ	73	ALA	BB	TCRα	49	ALA	BB	0.528	0.728	1.828	200
MHCβ	66	GLU	BB	TCRα	49	ALA	BB	0.706	0.806	2.006	200
MHCβ	73	ALA	BB	TCRα	29	ARG	BB	0.664	0.764	1.964	200
MHCβ	74	GLU	BB	TCRα	29	ARG	BB	0.625	0.725	3.825	200
MHCβ	76	ASP	BB	TCRα	65	LYS	BB	0.643	0.743	3.602	200
MHCβ	73	ALA	BB	TCRα	65	LYS	BB	0.930	1.030	4.130	200

Table 6: List of distance restraints between the TCR and the pMHC. Note that during the docking simulations the force constant was set to 1 kJ mol^{-1} nm^{-2}. A piecewise linear/harmonic restraint was used (bond type 10 in Gromacs) to keep the TCR and the pMHC together. The potential is quadratic for $r_{ij} < r_0$, 0 for $r_0 \leq r_{ij} < r_1$, quadratic for $r_1 \leq r_{ij} < r_2$ and linear for $r_2 \leq r_{ij}$.

Coarse graining and run parameters

Simulations were performed with the Martini 3 force field, version v.3.0.4.26 (Souza et al., 2021) in combination with a Gō-like model (Thallmair et al., 2019) (Poma et al., 2017). Coarse grained topologies were created using Martinize2 (Kroon, 2020). Simulations were performed with Gromacs, versions 2018-2022 (Abraham et al., 2015) with a 20 fs timestep and the 'New-RF' parameter set for the Martini force field (de Jong et al., 2016) with the modification that the Berendsen barostat was used. Temperature was kept at 310 K using the V-rescale thermostat (Bussi et al., 2007) using a coupling constant of τ_t = 1 ps. Pressure was semiisotropically coupled to an external bath of p = 1 bar with a coupling constant of τ_p = 4 ps and a compressibility of $\chi = 3 \times 10^{-4}$ bar^{-1} using the Berendsen barostat (Berendsen et al., 1984).

Simulation systems

The protein systems were embedded in POPC bilayers using the Insane script(Wassenaar et al., 2015). The TCR was embedded in a POPC bilayer of 1279 lipids (651 lipids in the extracellular leaflet and 628 lipids in the intracellular leaflet). The pMHC was embedded in a POPC bilayer of 1278 lipids (640 lipids in the extracellular leaflet and 638 lipids in the intracellular leaflet). The TCR only system was solvated in 90282 water beads (representing 361128 atomistic waters) and 1018 Na^+Cl^- beads were added (around 154 mM) and an additional 6 Cl^- ions to neutralize the system. The TCR-pMHC system was solvated in 95973 water beads (representing 383892 atomistic waters) and 1079 Na^+Cl^- beads were added (around 154 mM) and an additional 12 Na^+ ions to neutralize the system. One hundred independent 10 μs production simulations were

performed for both the TCR-only and TCR-pMHC systems. Note that each TCR-pMHC production run was preceded by a 1.5 μs preparatory simulation in which the TCR was slowly docked to the pMHC.

Analysis

The first 1 μs of each production simulation was discarded as equilibration, and the remaining (9 μs) trajectories were analyzed every 10 ns. The angle between the TCRβ EC and TM was calculated for simulation systems between the backbone beads of asparagine 97 serine 249 and valine 281 of the TCR β chain and for the cryo-EM structure between the Cα atoms of arginine 114, serine 268 and valine 300. Note that serine 249/268 and valine 281/300 are the corresponding residues in the simulation systems and cryo-EM structure, arginine 114 was chosen for its proximity to asparagine when superimposing simulated structure and the cryo-EM structure. Iso-occupancy maps were calculated using the Volmap tool in VMD. Grid spacing was set to 2 Å and counting of grid occupancy was performed after fitting the trajectories on the backbone beads of the TCR chains. Contacts between the TCR and CD3 chains were calculated with inhouse python scripts making use of the MDAnalysis library (Gowers et al., 2016; Michaud-Agrawal et al., 2011). Beads were considered in contact when their distance was < 6 Å, and residue contacts were calculated by summing all bead contacts. The following residues were considered to be part of the constant, variable, transmembrane and cytosolic domains for the TCR chains: TCRα variable: 1-106, constant: 107-198, transmembrane: 199-246, cytosolic: 247-249. TCRβ variable: 1-117, constant: 118-245, transmembrane: 246-285, cytosolic: 286-293. Trajectories were viewed using VMD and ChimeraX and pictures were rendered with ChimeraX (Humphrey et al., 1996; Goddard et al., 2018; Pettersen et al., 2021).

Bibliography

Abraham, Mark James, et al. (2015), 'GROMACS: High performance molecular simulations through multi-level parallelism from laptops to supercomputers', *SoftwareX*, 1 19-25.

Aivazian, D and LJ Stern (2000), 'Phosphorylation of T cell receptor zeta is regulated by a lipid dependent folding transition.', *Nat Struct Biol*, 7 (11), 1023-26.

Al-Aghbar, MA, et al. (2022), 'The interplay between membrane topology and mechanical forces in regulating T cell receptor activity.', *Commun Biol*, 5 (1), 40.
Alba, J, et al. (2020), 'Molecular Dynamics Simulations Reveal Canonical Conformations in Different pMHC/TCR Interactions.', *Cells*, 9 (4), E942.
Beddoe, Travis, et al. (2009), 'Antigen ligation triggers a conformational change within the constant domain of the αβ T cell receptor', *Immunity*, 30 (6), 777-88.
Bello, Martiniano and Jose Correa-Basurto (2016), 'Energetic and flexibility properties captured by long molecular dynamics simulations of a membrane-embedded pMHCII–TCR complex', *Molecular BioSystems*, 12 (4), 1350-66.
Berendsen, HJC, et al. (1984), 'Molecular dynamics with coupling to an external bath', *The Journal of Chemical Physics*, 81 (8), 3684-90.
Brameshuber, M, et al. (2018), 'Monomeric TCRs drive T cell antigen recognition.', *Nat Immunol*, 19 (5), 487-96.
Brazin, Kristine N, et al. (2018), 'The T Cell Antigen Receptor α Transmembrane Domain Coordinates Triggering through Regulation of Bilayer Immersion and CD3 Subunit Associations', *Immunity*, 49 (5), 829-841.e6.
Bussi, Giovanni, Davide Donadio, and Michele Parrinello (2007), 'Canonical sampling through velocity rescaling', *The Journal of Chemical Physics*, 126 (1), 014101.
Cai, Haogang, et al. (2018), 'Full control of ligand positioning reveals spatial thresholds for T cell receptor triggering', *Nature Nanotechnology*, 1-11.
Das, DK, et al. (2015), 'Force-dependent transition in the T-cell receptor β-subunit allosterically regulates peptide discrimination and pMHC bond lifetime.', *Proc Natl Acad Sci U S A*, 112 (5), 1517-22.
Davis, SJ and PA van der Merwe (2006), 'The kinetic-segregation model: TCR triggering and beyond.', *Nat Immunol*, 7 (8), 803-9.
de Jong, Djurre H, et al. (2016), 'Martini straight: Boosting performance using a shorter cutoff and GPUs', *Computer Physics Communications*, 199 1-7.
Dong, De, et al. (2019), 'Structural basis of assembly of the human T cell receptor–CD3 complex', *Nature*, 1-21.
Feng, Y., E. L. Reinherz, and M. J. Lang (2018), 'alphabeta T Cell Receptor Mechanosensing Forces out Serial Engagement', *Trends Immunol*, 39 (8), 596-609.
Fiser, András and Andrej Sali (2003), 'ModLoop: automated modeling of loops in protein structures', *Bioinformatics*, 19 (18), 2500-1.
Goddard, TD, et al. (2018), 'UCSF ChimeraX: Meeting modern challenges in visualization and analysis.', *Protein Sci*, 27 (1), 14-25.
Gowers, Richard J, et al. (2016), 'MDAnalysis: A Python package for the rapid analysis of molecular dynamics simulations', *Proceedings of the 15th Python in Science Conference*, 102-9.
Humphrey, William, Andrew Dalke, and Klaus Schulten (1996), 'VMD: Visual molecular dynamics', *Journal of Molecular Graphics*, 14 (1), 33-38.
Hwang, W, et al. (2020), 'The αβTCR mechanosensor exploits dynamic ectodomain allostery to optimize its ligand recognition site.', *Proc Natl Acad Sci U S A*, 117 (35), 21336-45.
Kim, S. T., et al. (2009), 'The alphabeta T cell receptor is an anisotropic mechanosensor', *J Biol Chem*, 284 (45), 31028-37.
Kroon, PC (2020), 'Automate, aggregate, assemble', (Dissertation, University of Groningen).

Lanz, AL, et al. (2021), 'Allosteric activation of T cell antigen receptor signaling by quaternary structure relaxation.', *Cell Rep*, 36 (2), 109375.
Lis, Mieszko, et al. (2011), 'Bridging the gap between single-template and fragment based protein structure modeling using Spanner', *Immunome Research*, 7 (1), 1.
Lo, Wan-Lin, et al. (2019), 'Slow phosphorylation of a tyrosine residue in LAT optimizes T cell ligand discrimination', *Nature Publishing Group*, 1-19.
Mariuzza, Roy A., Pragati Agnihotri, and John Orban (2020), 'The structural basis of T-cell receptor (TCR) activation: An enduring enigma', *Journal of Biological Chemistry*, 295 (4), 914-25.
Michaud-Agrawal, Naveen, et al. (2011), 'MDAnalysis: a toolkit for the analysis of molecular dynamics simulations.', *Journal of Computational Chemistry*, 32 (10), 2319-27.
Natarajan, Kannan, et al. (2017), 'An allosteric site in the T-cell receptor Cβ domain plays a critical signalling role', *Nature communications*, 8 (1), 1-14.
Newell, Evan W, et al. (2011), 'Structural basis of specificity and cross-reactivity in T cell receptors specific for cytochrome c-I-Ek', *Journal of immunology (Baltimore, Md.: 1950)*, 186 (10), 5823-32.
Nika, K, et al. (2010), 'Constitutively active Lck kinase in T cells drives antigen receptor signal transduction.', *Immunity*, 32 (6), 766-77.
Pandey, Prithvi R, et al. (2021), 'Structural variability and concerted motions of the T cell receptor-CD3 complex', *eLife*, 10
Pettersen, EF, et al. (2021), 'UCSF ChimeraX: Structure visualization for researchers, educators, and developers.', *Protein Sci*, 30 (1), 70-82.
Poma, Adolfo B, Marek Cieplak, and Panagiotis E Theodorakis (2017), 'Combining the MARTINI and Structure-Based Coarse-Grained Approaches for the Molecular Dynamics Studies of Conformational Transitions in Proteins', *Journal of Chemical Theory and Computation*, 13 (3), 1366-74.
Prakaash, D, et al. (2021), 'Multi-scale simulations of the T cell receptor reveal its lipid interactions, dynamics and the arrangement of its cytoplasmic region.', *PLoS Comput Biol*, 17 (7), e1009232.
Rangarajan, Sneha, et al. (2018), 'Peptide-MHC (pMHC) binding to a human antiviral T cell receptor induces long-range allosteric communication between pMHC- and CD3-binding sites.', *The Journal of biological chemistry*, 293 (41), 15991-6005.
Saito, Takashi and Tadashi Yokosuka (2006), 'Immunological synapse and microclusters: the site for recognition and activation of T cells', *Current Opinion in Immunology*, 18 (3), 305-13.
Schrödinger, LLC (2010), 'The PyMOL Molecular Graphics System, Version 1.7.0.0.',
Sokurenko, EV, V Vogel, and WE Thomas (2008), 'Catch-bond mechanism of force-enhanced adhesion: counterintuitive, elusive, but. widespread', *Cell Host Microbe*, 4 314-23.
Souza, PCT, et al. (2021), 'Martini 3: a general purpose force field for coarse-grained molecular dynamics.', *Nat Methods*, 1-7.
Thallmair, Sebastian, Petteri A Vainikka, and Siewert J Marrink (2019), 'Lipid Fingerprints and Cofactor Dynamics of Light-Harvesting Complex II in Different Membranes', *Biophysical journal*, 116 (8), 1446-55.
van der Merwe, PA and O Dushek (2011), 'Mechanisms for T cell receptor triggering.', *Nat Rev Immunol*, 11 (1), 47-55.

Wan, S, DR Flower, and PV Coveney (2008), 'Toward an atomistic understanding of the immune synapse: large-scale molecular dynamics simulation of a membrane-embedded TCR-pMHC-CD4 complex.', *Mol Immunol*, 45 (5), 1221-30.

Wassenaar, Tsjerk A, et al. (2015), 'Computational Lipidomics with insane: A Versatile Tool for Generating Custom Membranes for Molecular Simulations.', *Journal of Chemical Theory and Computation*, 11 (5), 2144-55.

Xu, C., et al. (2008), 'Regulation of T cell receptor activation by dynamic membrane binding of the CD3epsilon cytoplasmic tyrosine-based motif', *Cell*, 135 (4), 702-13.

Zhu, Cheng, et al. (2019), 'Mechanosensing through immunoreceptors', *Nature Publishing Group*, 1-10.

Zimmermann, Lukas, et al. (2018), 'A completely reimplemented MPI bioinformatics toolkit with a new HHpred server at its core', *Journal of molecular biology*, 430 (15), 2237-43.